

Torsional Interactions in Drivetrain System of Permanent Magnet Synchronous Generators Based Wind Farms

H. Y. Min (Student) and N. R. Watson (Faculty)

Department of Electrical and Electronics
University of Canterbury
New Zealand

Abstract-- Sub-synchronous torsional interaction (SSTI) can be an unstable condition that results in damage to the wind turbine (WT), permanent magnet synchronous generator (PMSG) or the drivetrain system. This condition is caused by an energy exchange between the electrical system and the mechanical drivetrain system. Sub-synchronous torsional interaction occurs when the wind turbine resonant frequency is near the complement of a torsional resonant frequency of the permanent magnet synchronous generator (PMSG). Under normal operating conditions, the WT and PMSG are controlled by adjusting their controller gain parameters to achieve steady-state conditions at their operating frequencies. When SSTI occurs in the drivetrain systems, the torque between the WT rotor and drivetrain may then get amplified, and potentially lead to the shaft failure and possible system outages. This paper looks at what is known as a type 4 (permanent magnet synchronous generators) wind energy conversion (WEC) system with a direct-drive drivetrain system.

Keywords: Permanent Magnet Synchronous Generator, Wind Turbine, Torsional Interaction, Torque Amplification, Torsional Torque, Subsynchronous Torsional Interaction

I. INTRODUCTION

Sub-synchronous torsional interaction (SSTI) in wind farms with Type 3 topology [1] associated with both series compensated transmission lines and STATCOM [2]-[4] and/or FACTS devices [5], [6] has been addressed in recent years [7], [8]. SSTI can be an unstable condition caused by an energy exchange between the electrical system and the mechanical drivetrain system [10]. SSTI can occur in any rotating system, but it is mainly critical for large rotating machines with low inherent damping properties. The mechanical damping coefficient and stiffness at the natural frequency of the drivetrain system are the critical parameters. This work is directly relevant to Type 4 (PMSG with full-scale converters) wind turbines with direct drive systems.

There are two frequencies in the vibration modes where the excitation occurs: resonant frequency and anti-resonant frequency. At the resonant frequency, the PMSG and the WT are in phase, resulting in the energy being built-up within the system instead of dissipating energy. For example, the WT rotor may not experience the oscillation while the PMSG

oscillates. The oscillation response of a torsional system such as the drivetrain system is influenced by i) the moment of inertia of the rotating masses, ii) the torsional stiffness of the flexible shafts and connected components and iii) the damping constant.

The objective of this paper is to investigate the SSTI and its effect on a large PMSG-based WEC system which is connected to the grid.

The paper is structured as follows: Section II outlines the drivetrain and PMSG of the WT modelling which includes drivetrain simulations. Section III demonstrates the time domain simulation of a WEC system to investigate the TI on the shaft which caused the system failure. Section VI qualitatively analyses the negative damping of the shaft system and Section V concludes the paper. Simulation parameters are presented in Appendix

II. SYSTEM MODELLING

For TI analysis of a multi-mass drivetrain system, the rotors of WT and the PMSG are treated as the contribution of rotating masses connected together by a spring represented by their damping and stiffness coefficient as shown in Fig. 1. Further details of SSTI and other relevant terms and definitions can be found in IEEE [10].

A. Two-Mass Model of Drivetrain System

The main focus is on investigating the effect of TI of large WEC systems. The shaft delivers the power from the wind turbine rotor to the PMSG rotor. An encoder monitors the actual position and speed of the WT rotor and the PMSG rotor. Typically, closed-loop feedback controllers are used to deliver optimal performance of the overall system. These controllers receive encoder information to send commands to amplifiers to control the pitch angle of the WT blades. In order to understand how the shaft system is affected by this process, the two-mass model shown in Fig. 1 is considered.

For this two-mass system shown in Fig. 1, a dynamic equation can be written in a second order differential equation derived from the torque equation, $T=I\cdot\alpha$. T is the torque, I is the rotational moment of inertia, and α is the angular acceleration of the shaft which is the second derivative of the angle. All the torques are calculated on one side of each mass.

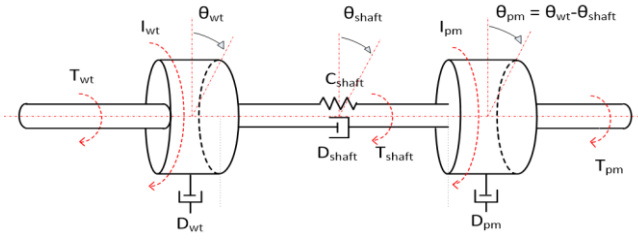


Fig. 1. Two-mass model of direct-drive drivetrain system.

The equation for the angular acceleration of the WT rotor is:

$$I_{wt} \cdot \frac{d^2\theta_{wt}}{dt^2} = T_{wt} - T_{shaft} - T_{wt,fr} \quad (1)$$

Also, the equation of instantaneous torque of wind turbine is given in [5]. Similarly, the equation for the PMSG the angular acceleration is given by:

$$I_{pm} \cdot \frac{d^2\theta_{pm}}{dt^2} = T_{shaft} - T_{pm} - T_{pm,fr} \quad (2)$$

However, there is no external torque applied to the PMSG. The only torque applied to the PMSG is the torque from the shaft and the counter electromagnetic torque from the PMSG itself. Therefore, $T_{pm} = 0$.

$$I_{pm} \cdot \frac{d^2\theta_{pm}}{dt^2} = T_{shaft} - T_{pm,fr} \quad (3)$$

The torque equation for the shaft and the friction are:

$$T_{shaft} = C_{shaft}(\theta_{wt} - \theta_{pm}) + D_{shaft} \left(\frac{d\theta_{wt}}{dt} - \frac{d\theta_{pm}}{dt} \right) \quad (4)$$

$$T_{wt,fr} = D_{wt} \left(\frac{d\theta_{wt}}{dt} \right) \quad (5)$$

$$T_{pm,fr} = D_{pm} \left(\frac{d\theta_{pm}}{dt} \right) \quad (6)$$

where I_{wt} , I_{pm} , T_{wt} , $T_{wt,fr}$, T_{shaft} , T_{pm} , $T_{pm,fr}$, C_{shaft} , D_{wt} , D_{pm} , D_{shaft} , θ_{wt} , θ_{pm} are the wind turbine rotor inertia [$\text{kg}\cdot\text{m}^2$], the generator inertia [$\text{kg}\cdot\text{m}^2$], the wind turbine torque [$\text{N}\cdot\text{m}$], the force of friction of wind turbine rotor [$\text{N}\cdot\text{m}$], the shaft torque [$\text{N}\cdot\text{m}$], the electromagnetic torque of PMSG in air gap [$\text{N}\cdot\text{m}$], the force of friction of PMSG [$\text{N}\cdot\text{m}$], the coefficient of shaft stiffness [$\text{N}\cdot\text{m}/\text{rad}$], the coefficient of wind turbine damping [$\text{N}\cdot\text{m}/\text{rad}/\text{s}$], the coefficient of PMSG damping [$\text{N}\cdot\text{m}/\text{rad}/\text{s}$], the coefficient of shaft damping [$\text{N}\cdot\text{m}/\text{rad}/\text{s}$], the position (angle) of wind turbine rotor [rad], the position (angle) of PMSG rotor [rad], respectively.

By substituting (4)-(6) to (1) & (3) the torque dynamic equations are obtained, yielding:

$$I_{wt} \cdot \frac{d^2\theta_{wt}}{dt^2} = T_{wt} - \left[C_{shaft}(\theta_{wt} - \theta_{pm}) + D_{shaft} \left(\frac{d\theta_{wt}}{dt} - \frac{d\theta_{pm}}{dt} \right) \right] - D_{wt} \left(\frac{d\theta_{wt}}{dt} \right) \quad (7)$$

$$I_{pm} \cdot \frac{d^2\theta_{pm}}{dt^2} = C_{shaft}(\theta_{wt} - \theta_{pm}) + D_{shaft} \left(\frac{d\theta_{wt}}{dt} - \frac{d\theta_{pm}}{dt} \right) - D_{pm} \left(\frac{d\theta_{pm}}{dt} \right) \quad (8)$$

where $\theta = \theta_{wt} - \theta_{pm}$ which is the displacement angle between

the WT rotor and PMSG rotor. Therefore $\dot{\theta}_{wt} - \dot{\theta}_{pm} = \dot{\theta}$ and $\ddot{\theta}_{wt} - \ddot{\theta}_{pm} = \ddot{\theta}$.

For the flexible shaft, the torsion which is related to the stiffness of the shaft material occurs when the shaft is subjected to a torque. Even though the torsion may be very small, it still makes the shaft twist, and one end rotates relative to the other end inducing shear stress on the shaft.

By rearranging (7) & (8), this system can be expressed as equations of motion, i.e.:

$$T_{wt} = I_{wt}\ddot{\theta}_{wt} + (D_{wt} + D_{shaft})\cdot\dot{\theta}_{wt} - D_{shaft}\dot{\theta}_{pm} + C_{shaft}\theta_{wt} - C_{shaft}\theta_{pm} \quad (9)$$

$$0 = I_{pm}\ddot{\theta}_{pm} + (D_{pm} + D_{shaft})\cdot\dot{\theta}_{pm} - D_{shaft}\dot{\theta}_{wt} - C_{shaft}(\theta_{wt} - \theta_{pm}) \quad (10)$$

This two degrees of freedom system still contains a fourth-order characteristic equation which will give a second-order polynomial. This polynomial will have complex solutions because the contribution of the damping on the shaft to the entire system.

By taking the Laplace transform of (9) & (10), the following transfer functions of the equations of motions in terms of the frequency are obtained.

$$\begin{bmatrix} T_{wt}(s) \\ 0 \end{bmatrix} = \begin{bmatrix} I_{wt}s^2 + (D_{wt} + D_{shaft})s + C_{shaft} & -(D_{shaft}s + C_{shaft}) \\ -(D_{shaft}s + C_{shaft}) & I_{pm}s^2 + (D_{pm} + D_{shaft})s + C_{shaft} \end{bmatrix} \begin{bmatrix} \theta_{wt}(s) \\ \theta_{pm}(s) \end{bmatrix} \quad (11)$$

The term D_{wt} and D_{pm} are coupled with D_{shaft} contributing the damping oscillation in the system. These terms are called cross-coupled damping [12]. When there is a positive cross-coupled damping, a deflection will cause a reaction force as displacing the shaft horizontally on applying a vertical force. If these damping coefficients are large enough to make the mechanical system unstable, the both the WT and the PMSG need to be shut down immediately. The damping effect of the WT and PMSG on the resonant frequencies is negligible [16] as (12) & (13) shows.

$$\omega_{AR} = \sqrt{\frac{C_{shaft}}{I_{pm}}} \quad (12)$$

$$\omega_R = \sqrt{C_{shaft} \left(\frac{I_{wt} + I_{pm}}{I_{wt}I_{pm}} \right)} \quad (13)$$

Then, (11) becomes:

$$\frac{\theta_{wt}(s)}{T_{wt}(s)} = \frac{1}{(I_{wt} + I_{pm})s^2} \left[\frac{I_{wt}s^2 + D_{shaft}s + C_{shaft}}{\frac{I_{wt}I_{pm}}{I_{wt} + I_{pm}}s^2 + D_{shaft}s + C_{shaft}} \right] = \frac{K \left[\frac{s^2}{\omega_{AR}^2} + \frac{2\zeta_{AR}s}{\omega_{AR}} + 1 \right]}{s^2 \left[\frac{s^2}{\omega_R^2} + \frac{2\zeta_{AR}s}{\omega_R} + 1 \right]} \quad (14)$$

$$\frac{\theta_{pm}(s)}{T_{wt}(s)} = \frac{1}{(I_{wt} + I_{pm})s^2} \left[\frac{D_{shaft}s + C_{shaft}}{\frac{I_{wt}I_{pm}}{I_{wt} + I_{pm}}s^2 + D_{shaft}s + C_{shaft}} \right]$$

$$= \frac{K(\tau s + 1)}{s^2 \left[\frac{s^2}{\omega_R^2} + \frac{2\zeta_R s}{\omega_R} + 1 \right]} \quad (15)$$

where

$$K = \frac{1}{I_{wt} + I_{pm}} \quad \tau = \frac{D_{shaft}}{C_{shaft}}$$

$$\zeta_{AR} = \frac{D_{shaft}}{2\sqrt{C_{shaft}I_{pm}}} \quad \zeta_R = \frac{D_{shaft}}{2\sqrt{C_{shaft}\left(\frac{I_{wt}I_{pm}}{I_{wt} + I_{pm}}\right)}}$$

The frequencies, ω_{AR} and ω_R are the oscillation modes where the interaction between WT and PMSG occurs. ω_{AR} and ω_R are the anti-resonant frequency and the resonant frequency respectively.

The peaks of ω_{AR} and ω_R of the system shown in Fig. 2(b) are the frequencies that the WT system exhibits resonant behaviours. At ω_{AR} , the PMSG rotates with an equal and opposite torque from the WT rotor resulting the PMSG rotor starts oscillating. It means that the exciting force of oscillations from the WT is “absorbed” [17] by physically coupled components such as the shaft and the PMSG rotor. The coupled components behave as an additional restraint to the system at the anti-resonant frequency.

At ω_R , the WT and PMSG rotors are at the peak of the resonant frequency, thus the energy from the WT and PMSG become amplified in the drivetrain system resulting both WT and PMSG rotors oscillate. The problems of both ω_{AR} and ω_R are 1) the PMSG or the shaft oscillation may be undetected, and 2) the rotating system with feedback controls will likely get damaged. For example, the overall system may operate well in the steady-state condition, but the WT and PMSG may fail to operate due to a sudden change (i.e. rotational speed) if the oscillation is not detected in a timely manner.

B. Drivetrain Response Simulation

The system was simulated with MATLAB[®] with actual data given in Appendix A. Two different cases were simulated: a flexible shaft (Fig. 2) and an infinitely rigid shaft (Fig. 3).

As the simulation result in Fig. 2 depicts, the peaks of anti-resonance and resonance can potentially interfere with the feedback control tuning. Practically the PMSG feedback controller is tuned by adjusting the controller gain parameters to achieve steady-state conditions around the operating frequency. Typically, placing a low-pass filter would remove these peaks. However, Fig. 2 shows that both anti-resonance and resonance occur at very low frequencies. Placing a low-pass filter to cut off these would require a low cut-off frequency which would reduce the usable frequency bandwidth. As the inertia ratio increases, both anti-resonant and resonant peaks are attenuated. More importantly, they are shifted to higher frequencies. Also, the stiffness of the shaft can tie the peaks of anti-resonant and the resonant closer together.

The equations for ω_{AR} and ω_R show that the resonant

frequency is strongly influenced by the stiffness of the shaft, the inertia of PMSG and WT. Fig. 3 shows that stiffer shaft alone can significantly improve the damping response in the drivetrain system. Also, the problematic anti-resonant and resonant peaks are adequately attenuated. However, this simulation does not show how the drivetrain will interact with other components such as the WT and the PMSG.

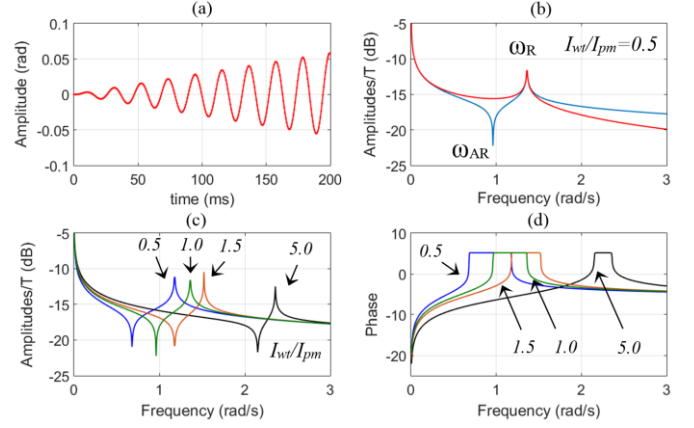


Fig. 2. Drivetrain simulation result with a flexible shaft: (a) Step response of shaft damping, (b) bode magnitude plot of θ_{wt}/T_{wt} and θ_{pm}/T_{pm} , (c) bode magnitude plot of θ_{wt}/T_{wt} with different inertia ratios and (d) phase plot of WT and PMSG.

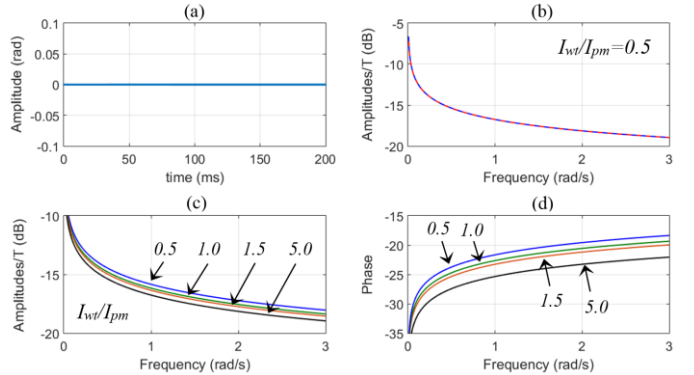
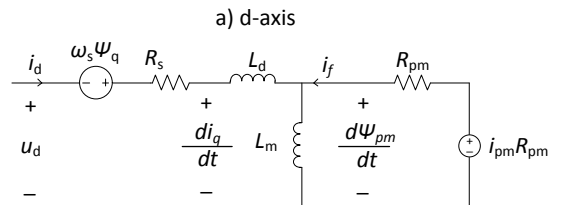


Fig. 3. Drivetrain simulation result with a rigid shaft: (a) Step response of shaft damping, (b) bode magnitude plot of θ_{wt}/T_{wt} and θ_{pm}/T_{pm} , (c) bode magnitude plot of θ_{wt}/T_{wt} with different inertia ratios and (d) phase plot of WT and PMSG.

C. Permanent Magnet Synchronous Generator Model

The following equivalent circuit of PMSG, shown in Fig. 3, is based on the transient model of permanent magnet synchronous machine (PMSM). Any change in the magnetic flux of the rotor magnet will cause an induced electromotive force (EMF) which results in a circulating current in the magnet.



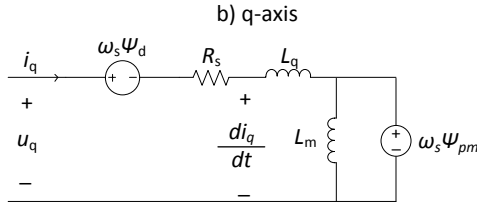


Fig. 4. PMSG circuit representation: (a) d-axis and (b) q-axis circuits.

Sebastian *et. al.* [4] stated that “assuming that the penetration depth δ at the maximum frequency of concern is large in comparison with the magnet’s radial thickness, each magnet can be considered approximately as a conducting loop of length l , angular span 2α , having a resistance R'_m .” When transferred across the air gap to the equivalent number of direct-axis stator turns, this can be represented as a resistance R_m , connected across the direct-axis magnetizing inductance L_m .

$$R_m = \left(\frac{4N_s}{\pi \sin(\alpha)} \right)^2 \frac{R'_m}{n} \quad (16)$$

where n is the number of poles and N_s is the number of turns in the stator winding.

Since the magnet-to-core interface is mainly a non-conducting adhesive, this path can be ignored [4]. Based on the circuit model with no zero-sequence components present, the equation of voltage in d-q axis can be expressed as:

$$u_d = R_s i_d - \omega_s \psi_q + (L_d + L_m) \frac{di_d}{dt} \quad (17)$$

$$u_q = R_s i_q + \omega_s \psi_d + (L_q + L_m) \frac{di_q}{dt} + \omega_s \psi_{pm} \quad (18)$$

where $\psi_d = (L_d + L_m) \cdot i_d$ and $\psi_q = (L_q + L_m) \cdot i_q$

Substitute ψ_d and ψ_q to (15) and (16) respectively to

obtain the current dynamics in state form as the following.

$$\frac{di_d}{dt} = \frac{u_d - R_s i_d + \omega_s (L_q + L_m) i_q}{(L_d + L_m)} \quad (19)$$

$$\frac{di_q}{dt} = \frac{u_q - R_s i_q - \omega_s (L_d + L_m) i_d - \omega_s \psi_{pm}}{(L_d + L_m)} \quad (20)$$

where ω_s , R_s , ψ_{pm} , ψ_d , ψ_q , L_d , L_q , L_m and R_m are the synchronous rotor speed of PMSG [rad/s], the stator resistance [ohm], the flux linkage by permanent magnet [Wb], the flux linkage of d-axis [Wb], the flux linkage of q-axis [Wb], the inductance of d-axis [H], the inductance of q-axis [H], the stator mutual inductance [H] and stator mutual resistance [H] respectively.

The electromagnetic torque, T_{pm} [Nm] of the PMSG is calculated as the following.

$$T_{pm} = 1.5n[\psi_{pm} i_q + (L_d - L_q) i_d i_q] \quad (21)$$

Ideally, T_{pm} should be equal and opposite of the T_{wt} in (1) i.e. $T_{wt} - T_{pm} = 0$ if the losses in the drivetrain system is negligible.

D. Blade Pitch, Torque and Generator-Side Converter Controls

There are numerous generator torque controllers in use, however, many of these are proprietary. This work uses the genetic wind turbine pitch control and torque control algorithms given in [7], with slow resonant controller tuning techniques used in [8], which are directly implemented for the low speed WT.

The torque control of the generator is achieved by setting the torque, T_{pm} , i.e.

$$T_{pm} = K \omega_s^2 \quad (22)$$

where K is given by [8]

$$K = \frac{1}{2} \rho \pi R^5 \left(\frac{C_{p_max}}{\psi_{pm}^2} \right) \quad (23)$$

where C_{p_max} , R , ρ and λ^* are the maximum achievable power coefficient by WT, the rotor radius or the blade length [m], the air density [kg/m³], and the tip-speed-ratio at C_{p_max} , respectively.

The generator control design was based on the assumption that the d-axis is perfectly aligned with ψ_{pm} . The q-axis current is used to control the electromagnetic torque of the PMSG. Thus, reference d-axis current i_d^* is set to zero, whereas the reference q-axis current i_q^* was computed as:

$$i_q^* = \frac{2}{3n\psi_{pm}} T_{pm}^* \quad (24)$$

Due to space limitations the details of the grid-side converter control is not given.

E. WEC System Simulation Results

MATLAB/Simulink[®] is used to simulate the model in time domain.

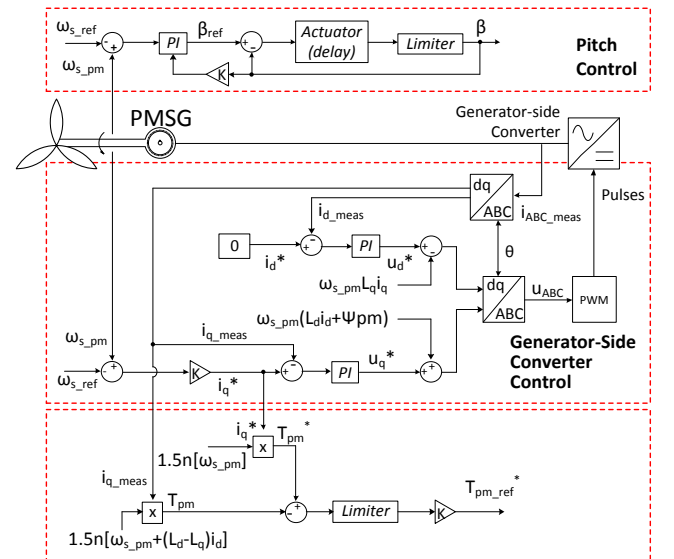


Fig. 5. Control block diagram based on (15) to (22)

Case 1: flexible shaft

The WT system was simulated with the flexible shaft

parameters given Appendix to obtain the steady state condition. The stiffness coefficient of the flexible shaft is obtained from a real system. The results of Case 1 are given in Fig 6 & 7.

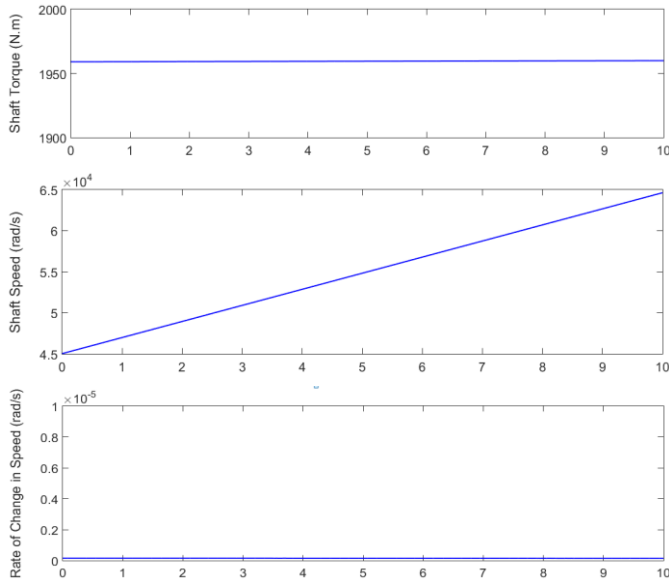


Fig. 6. Torque, speed and derivative of speed of the shaft in time (s)

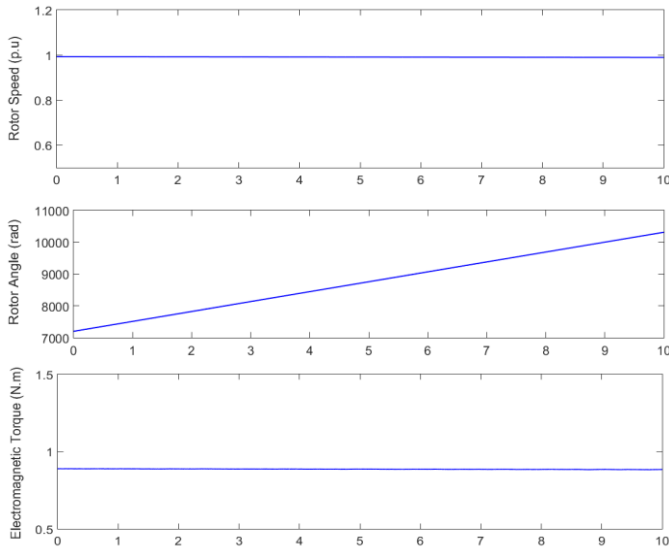


Fig. 7. Speed, angle and EM torque of the PMSG in time (s)

Case 2: rigid shaft

The stiffness coefficient of the rigid shaft is given in Appendix that perfectly attenuates both anti-resonant and resonant peaks shown in Fig 3. The stiffness coefficient of the flexible shaft is then replaced with the stiffness coefficient of the rigid shaft after Case 1. The results of Case 2 are given in Fig. 8 & 9.

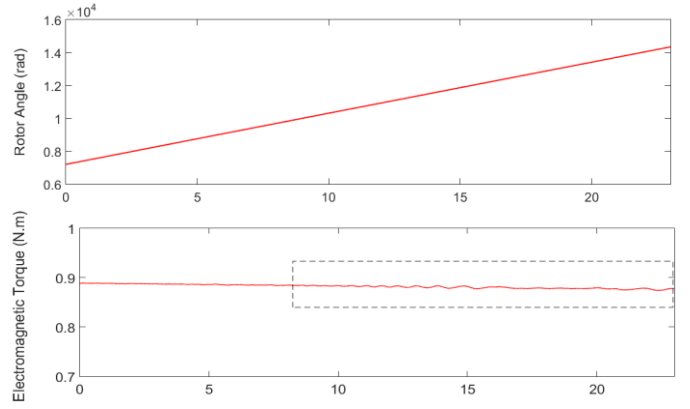
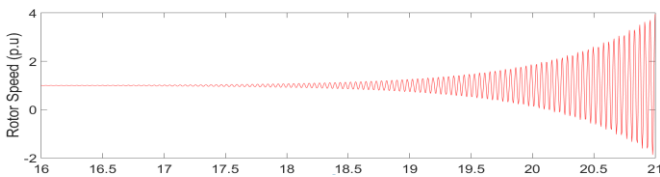


Fig. 8. Speed, angle and EM torque of the PMSG in time (s)

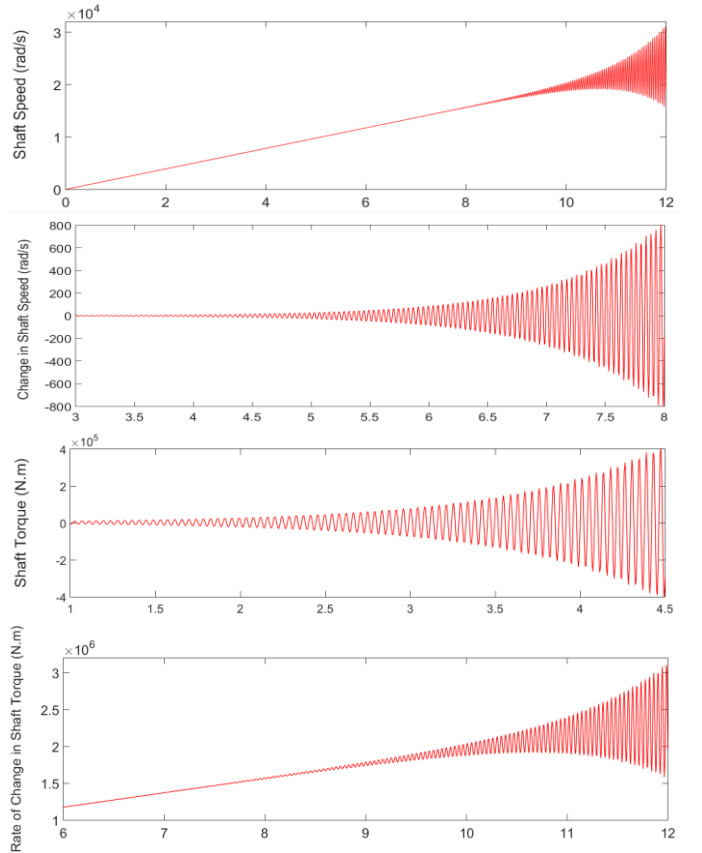


Fig. 9. Speed, rate of change in speed, torque ($T_{sh}=T_{wt}-T_{pm}$) and derivative of the torque of the shaft in time (s)

III. ANALYSIS OF NEGATIVE DAMPING

The simulation results shown in Fig. 6-9 depict the torsional interaction between the shaft and the PMSG which led the system unstable. As shown in Fig. 1, the coupling torque on the shaft, T_{shaft} is given in (4). From Fig. 3(a) the damping response with the rigid shaft is negligible. Thus, T_{shaft} is determined by the angular displacement between the WT and PMSG rotors;

$$T_{shaft} = C_{shaft}(\theta_{wt} - \theta_{pm}) \quad (25)$$

Assuming that the friction of the WT and PMSG is negligible, (1) & (3) become,

$$I_{wt} \cdot \frac{d^2\theta_{wt}}{dt^2} = T_{wt} - T_{shaft} \quad (26)$$

$$I_{pm} \cdot \frac{d^2\theta_{pm}}{dt^2} = T_{shaft} \quad (27)$$

Defining $\theta = \theta_{wt} - \theta_{pm}$, subtracting (27) divided by I_{pm} from (26) divided by I_{wt} gives,

$$\frac{d^2\theta}{dt^2} = \frac{1}{I_{wt}} \cdot T_{wt} - \frac{1}{I_{wt}} \cdot T_{shaft} - \frac{1}{I_{pm}} \cdot T_{shaft} \quad (28)$$

By substituting (25) to (28) the following equation is obtained.

$$I_{pm} \cdot \frac{d^2\theta}{dt^2} = \frac{1}{I_{wt}} \cdot T_{wt} - \frac{I_{wt} + I_{pm}}{I_{wt} I_{pm}} \cdot C_{shaft} \theta \quad (29)$$

For steady state operation, the WT rotor torque can be expressed as a function of the WT rotor speed,

$$T_{wt} = f_{T_{wt}} \left(\frac{d\theta_{wt}}{dt} \right) \quad (30)$$

During torsional interaction between the WT and PMSG rotors, the oscillating component of the larger inertia will less likely experience the instability by the torsional torque. Therefore, the PMSG is referred as the system average of the mechanical synchronous speed of the system,

$$\begin{aligned} \frac{d\theta_{wt}}{dt} &= \frac{d\theta_{pm}}{dt} + \frac{d\theta}{dt} \\ &= \omega_{pm} + \frac{d\theta}{dt} \end{aligned} \quad (31)$$

For analysing the limit of the system, Taylor series expansion was used. Considering only the first term, the function $f_{T_{wt}}(\omega_{wt})$ at the point ω_{pm} is expressed as:

$$\frac{d^2\theta}{dt^2} - \frac{\eta}{I_{wt}} \frac{d\theta}{dt} + \frac{I_{wt} + I_{pm}}{I_{wt} I_{pm}} \cdot C_{shaft} \theta = \frac{1}{I_{wt}} f_{T_{wt}} \left(\frac{d\theta_{wt}}{dt} \right) \quad (32)$$

Where η is the rate of change of torque-speed curve of the PMSG which is not the same as the torque-speed curve of the WT. Then the eigenvalues of the shaft is the following.

$$\lambda_{shaft} = \frac{\frac{\eta}{I_{wt}} \pm j \sqrt{-\left(\frac{\eta}{I_{wt}}\right)^2 + 4 \cdot \frac{I_{wt} + I_{pm}}{I_{wt} I_{pm}} \cdot C_{shaft}}}{2} \quad (33)$$

If η is positive, the first term is positive. This indicates that the eigenvalues will be on the right-half of the complex plane. Thus, the shaft will undergo negative damping and the increase the response of the torsion shown in Fig. 8 & 9. From (33), the unstable torsional oscillation can be identified in frequency domain.

$$f_{shaft_osc} = \frac{1}{4\pi} \pm j \sqrt{-\left(\frac{\eta}{I_{wt}}\right)^2 + 4 \cdot \frac{I_{wt} + I_{pm}}{I_{wt} I_{pm}} \cdot C_{shaft}} \quad (34)$$

Since η is the rate of change of torque-speed, the first term under the square root of (34) is much smaller than the second term. Therefore, I_{wt} and C_{shaft} will dictate the oscillation frequency. If $I_{pm} > I_{wt}$, I_{pm} and C_{shaft} will dictate the oscillation frequency of the system. In either case, the stiffness of the shaft is always the dictating parameter. In addition, η is useful in torque control design of the PMSG. From (23), assuming the rotor flux linkage is constant, the mechanical torque of the

PMSG rotor only depends on the speed of the PMSG. As shown in Fig. 8, the indication of the growth of oscillation can be seen by monitoring the rate of change in variable η shown in Fig. 10.

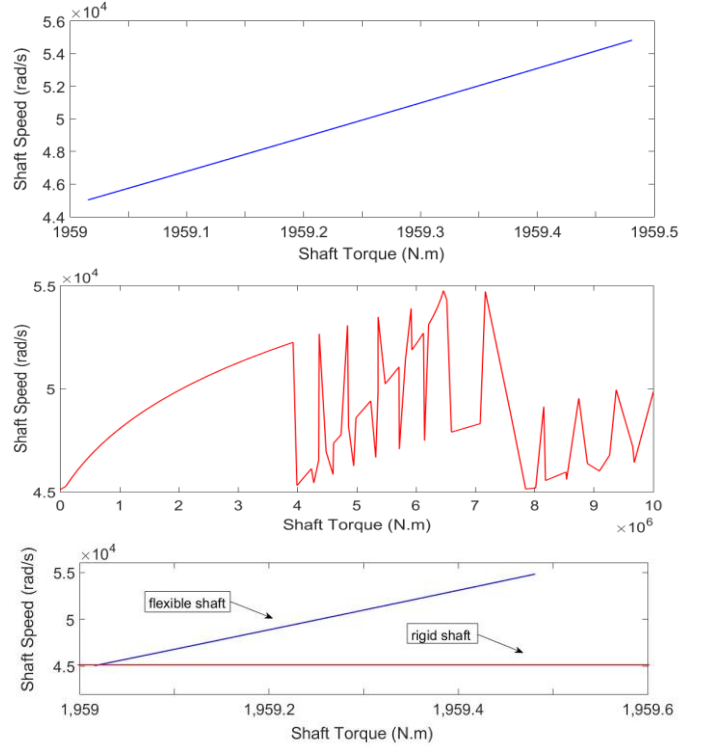


Fig. 10. Torque-speed curve (flexible shaft), torque-speed curve (rigid shaft) and torque-speed curve of flexible shaft vs. rigid shaft (around steady state operating point).

IV. CONCLUSIONS

This paper investigated the TI behaviour of a direct-drive PMSG based WEC system using time domain simulation conducted in MATLAB & SIMULINK®. The torsional oscillation simulation has been conducted for a particular Type-4 WEC system to analyse the negative damping response of the drivetrain system with a nearly infinite stiffness of the shaft. It is observed that the torsional mode not only exists with the drivetrain system with a flexible shaft, but also it does with the shaft with nearly infinite stiffness.

It is shown that when η is positive and large, the system will result in negative damping and the increase the response of the torsion on the shaft. As shown in Fig. 10, the speed of the shaft is nearly insensitive to the change in torque. However, the oscillation of the shaft quickly builds up and exhibit negative damping which leads to system instability. However, if η is positive but very small (close to zero), the growth rate of the oscillation of the shaft system may be slower, but it will eventually lead to an unstable system condition after some period of time.

It is shown in this paper that the negative damping behaviour on the drivetrain system can be occurred due to the shaft stiffness resulting a strong coupling between the rotating masses and the stiffness of the shaft system. The resulting

oscillation in the shaft is large enough to make the system unstable in this particular WEC system. The simulation showed that sustained torsional oscillations may result in catastrophic failure of the entire system.

In short, this paper emphasises the importance of the complete system, not only its individual component. The interaction (i.e. the SSTI in the shaft shown in the paper) between the electrical and mechanical components often neglected from the system design level.

V. APPENDIX

DAMPING PARAMETER CALCULATIONS:

$$K = \frac{1}{8.2 \times 10^6} \quad \tau = 5.28 \times 10^{-4} \quad \zeta_{AR} = 3.435 \times 10^{-4}$$

$$\zeta_R = 4.295 \times 10^{-4} \quad \omega_{AR} = 1.302 \text{ rad/s} \quad \omega_R = 1.6267 \text{ rad/s}$$

$$\omega_d = \omega_R \sqrt{1 - \zeta_R} = 1.6264 \text{ rad/s}$$

TABLE I
PMSG PARAMETERS (ROUND ROTOR TYPE)

Parameters	Value	Unit
MVA Rating	2.25	MVA
Rated Power	2	MW
Terminal Voltage	690	V
Rated Stator Current	1870	A
Efficiency	92	%
Rated Speed	23.5	rpm
Pole Pairs	18 (20 slots)	
Inertia	3.47×10^6	$\text{kg} \cdot \text{m}^2$
Viscous Damping	0.1	$\text{N} \cdot \text{m} \cdot \text{s}$
Static Friction	0	$\text{N} \cdot \text{m}$
Flux Linkage	1.742	$\text{V} \cdot \text{s}$
Stator Resistance	1.85	$\text{m}\Omega$
Armature Inductance ($L_d=L_q$ [9])	0.285	mH

TABLE II
WT PARAMETERS

Parameters	Value	Unit
Blade Length	37.5	m
Inertia	6.34×10^6	$\text{kg} \cdot \text{m}^2$
Viscous Friction	0.1	$\text{N} \cdot \text{m} \cdot \text{s}$
Wind Speed	12.5	m/s

TABLE III
DRIVETRAIN PARAMETERS

Parameters	Value	Unit
Stiffness	5.87×10^6 (flexible)	$\text{N} \cdot \text{m}$
	6.20×10^{10} (rigid)	
Damping	3.1×10^3	$\text{N} \cdot \text{m} \cdot \text{s}$

VI. REFERENCES

[1] G. D. Irwin, "Sub-Synchronous Interactions with Wind Turbines," Technical Conference – CREZ System Design and Operation, January 26, 2010, Taylor, Texas, USA. Available: http://www.ercot.com/content/meetings/other/keydocs/2014/1119-PROJECT4350/AnalysisMethods_SSR_SSCI_SSTI.ppt

[2] J. Zhang, X. Xiao, P. Zhang, C. Luo, Y. Wu, J. Lu, L. Ren, "Suppressing Intermittent Subsynchronous Oscillation via

Subsynchronous Modulation of Reactive Current", *Power Delivery IEEE Trans.*, vol. 30, pp. 2321-2330, 2015

[3] G. D. Irwin, A. Isaacs and D. Woodford, "Simulation Requirements for Analysis and Mitigation of SSCI Phenomena in Wind Farms," Transmission and Distribution Conference and Exposition, 2012 IEEE PES, 2012, pp. 1-4.

[4] T. S. Bi, Y. L. Kong and S. W. Xiao, "Review of Sub-synchronous Oscillation with Large-scale Wind Power Transmission," *Journal of Electric Power Science and Technology*, Vol. 27, No. 1, 2012, pp. 10-15

[5] W. Gu, X. Y. Li, Y. H. Wang, Z. L. Mu and W. Wei, "Mitigation Effects of UPFC on Sub-synchronous Oscillation in a Wind Farm," *Automation of Electric Power Systems*, Vol. 34, No. 8, 2010, pp. 101-105.

[6] R. K. Varma, S. Auddy, Y. Semsedini, "Mitigation of Subsynchronous Resonance in a Series-Compensated Wind Farm Using FACTS Controllers," *IEEE Trans. on Power Delivery*, 2008, pp. 1645-1654

[7] H. Chen, C. Guo, J. Xu, P. Hou, "Overview of Sub-synchronous Oscillation in Wind Power System," *Energy and Power Engineering*, vol. 5, pp. 454-457, 2013

[8] X. L. Liu, "Analysis of Major Types of Wind Turbines and the Application of Technology," *Electrical Manufacturing*, 2009, pp. 18-20.

[9] Z. Lubosny, *Wind Turbine Operation in Electric Power Systems*, Springer, 2006

[10] IEEE Committee Report, "Terms, Definitions and Symbols for Subsynchronous Oscillations," *IEEE Trans. On Power Apparatus and Systems*, vol. PAS-104, no. 6, pp. 1326-1334, June 1985

[11] T. Sebastian and G. R. Slemon, "Transient modeling and performance of variable-speed permanent-magnet motors." *IEEE Transactions on Industry Applications*, vol. 25.1, pp. 101-106, 1989.

[12] L. W. Cai, *Fundamentals of Mechanical Vibrations*, John Wiley & Sons, 2016, p. 307-313

[13] M. H. Hansen, A. Hansen, T. J. Larsen, S. Øye, P. Sørensen, and P. Fuglsang, "Control design for a pitch-regulated, variable speed wind turbine," Risø National Laboratory, Roskilde, Denmark, Tech. Rep. Risø-R-1500(EN), Jan., 2005.

[14] L. Y. Pao and K. E. Johnson, "A Tutorial on the Dynamics and Control of Wind Turbines and Wind Farms," *Proc. Amer. Ctrl. Conf.*, June 2009.

[15] K. Sugiura, and Y. Hori, "Vibration suppression in 2-and 3-mass system based on the feedback of imperfect derivative of the estimated torsional torque." *IEEE Trans. On Indus. Elect.*, vol 43, no. 1, pp. 56-64, 1996.

[16] J. S. Rao, *Rotor dynamics*, New Age International, pp. 37-40, 1996.

[17] F. Wahl, G. Schmidt, and L. Forrai, "On the Significance of Antiresonance Frequencies in Experimental Structural Analysis", *Journal of Sound and Vibration*, vol. 219(3), pp. 379–394, 1999.